MĀPAN-Journal of Metrology Society of India (September 2013) 28(3):205–215
DOI 10.1007/s12647-013-0068-7

ORIGINAL PAPER

The Effect of Nanoparticle Morphology on the Measurement Accuracy of Mobility Particle Sizers

A. Awasthi[1], B.-S. Wu[1], C.-N. Liu[1], C.-W. Chen[2], S.-N. Uang[2] and C.-J. Tsai[1]*

[1]Institute of Environmental Engineering, National Chiao Tung University, Hsinchu 300, Taiwan

[2]Institute of Occupational Safety and Health, Council of Labor Affairs, Taipei 221, Taiwan

Received: 15 July 2013 / Accepted: 26 August 2013 / Published online: 20 September 2013

Abstract: The influence of particle morphology on the accuracy of nanoparticle size distributions measured by the engine exhaust particle sizer spectrometer (EEPS, TSI Model 3090) was studied using the scanning mobility particle sizer (SMPS, TSI Model 3936) as a reference. The EEPS shows higher total number concentrations with the maximum relative difference up to 67 % and smaller number median mobility diameters for polydisperse silver nanoparticles generated in the laboratory. To provide a quantitative explanation of the difference, generated polydisperse nanoparticles were classified as monodisperse particles with the initial equivalent mobility diameter (d_{m1}) and sintered in the second furnace at different temperatures (room temperature to 600 °C), to change their morphologies for the comparison tests. Without sintering (room temperature), results show that the measured mobility diameter (d_{m2}) of the EEPS is smaller than that measured by the SMPS when d_{m1} is larger than 30 nm and the difference increases as d_{m1} is increased from 30 to 300 nm. But the difference decreases as the morphology of particles is changed from branched chain agglomerates to spheres for d_{m1} less than 80 nm and the sintering temperature higher than 200 °C. Theoretical analysis shows that the mean charge per agglomerates is more than that of spheres resulting in overestimation of the electrical mobility and underestimation of the d_{m2} by the EEPS.

Keywords: Aerosol measurement; Particle sizer; Electrical mobility analyzer; Sizing accuracy

1. Introduction

Association of the exposure of ultrafine particles or nanoparticles with the adverse health effects was observed in many previous studies [1–3]. Therefore, the accurate assessment of nanoparticle exposure is very important, in which the number concentration distribution is one of the most frequently used measurement parameters as there are many real time instruments that are commercially available. However, atmospheric and engineered nanoparticles are often non-spherical [4], such as soot agglomerates and engineered silver, zinc oxide, and titanium dioxide nanoparticles [5, 6], whose morphology can affect the accuracy of the number distribution measurement.

Different aerosol instruments have been developed using various techniques [7]. The most widely used technique for nanoparticle and submicron particle measurements is the particle electric mobility (Z_p) method [8] which was initially developed to measure ion in gases [8, 9]. Since then, numerous studies have been conducted to improve this technique such that the instruments are now capable of measuring the size distributions of aerosol particles ranging from 2.5 to 1,000 nm. Instruments based on Z_p are generally termed as mobility particle sizers, which mainly consist of three components: a particle charger, a mobility classifier and a signal detector. The particle charger could either be a bipolar or unipolar diffusion charger. The bipolar diffusion charger (also called the electrostatic neutralizer) uses a radioactive source to charge the aerosols. One of the instruments that uses the bipolar charger is the SMPS, which is widely used to measure nanoparticle size distributions [10–14]. The Fast Mobility Particle Sizer (FMPS) and EEPS are the examples which use the unipolar charger, and its charging efficiency can be higher than that of the bipolar charger also it eliminates the use of radioactive sources [15–19]. The SMPS is accurate in sizing but it takes

*Corresponding author, E-mail: cjtsai@mail.nctu.edu.tw

30 s or longer to measure a particle size distribution. Due to its slow scanning speed relative to the transient nature of aerosols produced during the vehicle operation, the application of the SMPS to vehicular emissions is limited. In comparison, the EEPS is used for engine exhaust particle size measurement due to its fast time resolution of 0.1 s and the FMPS is used in non-engine application that require fast response with 1 s time resolution. More details of SMPS, FMPS and EEPS are shown in Table 1.

Several studies showed that measured data varied significantly from one instrument to another [20–24]. Kaminski et al. [20] compared 24 aerosol instruments including 11 electrical mobility based devices for the measurement of particle number size distributions (5 Grimm SMPS+C, 3 TSI SMPS and 3 FMPS), 12 instruments for the measurement of size-integrated number or lung deposited surface area concentrations and 1 TSI ultrafine condensation particle counter (CPC). The FMPSs showed the discrepancies on the order of ±25 % for sizing and ±30 % for total concentrations in comparison to a freshly calibrated Grimm SMPS. The comparison was the best for compact NaCl particles with sizes around 40 nm and the worst for larger Di-Ethyl-Hexyl-Sebacate and agglomerated soot particles. It was also found that the agreement was better for 60 nm than that for 100 nm soot particles. Therefore it was concluded that both particle size and morphology is responsible for the measurement difference between FMPS and SMPS.

Asbach et al. [21] compared 4 mobility sizers which include a TSI FMPS, a Grimm SMPS+C, and 2 TSI SMPSs and found that the size distributions measured by the FMPS always shifted toward smaller sizes for both soot and NaCl nanoparticles. The same results were shown by Leskinen et al. [22] that the FMPS had a smaller number median diameter (NMD) for TiO_2 agglomerates than that of the TSI SMPS but the NMDs of both FMPS and SMPS were in good agreement with each other for ammonium sulfate particles which are spherical in shape in comparison to TiO_2. Joeng and Evans [23] investigated the performance of two TSI SMPSs and two FMPSs by using ambient nanoparticles as well as engineering nanoparticles. Comparable results of particle size distributions were only obtained for salt and gold particles [23]. In these previous studies, no quantitative explanation is given for the reason of NMD underestimation by the FMPS in comparison to the SMPS.

Previous studies showed that particle morphology is an important factor which affects the unipolar charging process [24, 25]. Frank et al. [26] proposed that there is a need to study the effect of particle morphology on the measurement difference among SMPS, the electrical aerosol detector and CPC. Aggregates and spherical particles with the same mobility diameter show similar bipolar diffusion charging characteristic in the transition regime [27]. It is observed that if aggregate and spherical particles have the same mobility diameter, then both will have a similar projected area diameter [28], but aggregates have a larger geometric surface area [29]. In bipolar charging, the charging mechanism is mainly governed by the diffusion between particles and ions and not by other forces such as the electrostatic force between charged particles and ions. Thus the effect of particle shape is not significant to bipolar diffusion charging. However, the particle shape would be expected to play an important role in unipolar diffusion charging because highly charged particles create a great deal of electrostatic force between charged particles and ions comparable to diffusion force. Chang [30] proposed equations for calculating the mean charge per particle of arbitrary shape. Oh et al. [31] found that TiO_2 agglomerates had 30 % more charge than that of spherical particles. Shin et al. [32] developed a new model to estimate the electrical capacitance of loose agglomerates ($C_{p,agg}$) and found it was much larger than that of the spheres with the same mobility diameter. As a result, loose agglomerates acquired higher mean charge per particle compared to compact particles.

From the above review, it is seen that most of the studies focused on the comparison of the FMPS with the other

Table 1 Specifications of the SMPS, FMPS and EEPS

	SMPS, TSI 3936	FMPS, TSI 3091	EEPS, TSI 3090
Particle size range (nm)	2.5–1,000	5.6–560	5.6–560
Particle size resolution	64 Channels per decade	16 Channels per decade (32 total)	16 Channels per decade (32 total)
Particle detector	UWCPC	Electrometers	Electrometers
Electrometer channels	NA	22	22
Charging type	Neutralizer	Corona charger	Corona charger
Charging method	Bipolar	Unipolar	Unipolar
Concentration range (particle/cm^3)	1–10^7	100–10^7 (5.6 nm)	300–10^7 (5.6 nm)
		1–10^5 (560 nm)	3–10^5 (560 nm)
Time resolution	30–120 s	1 Size distribution/s	10 Size distribution/s
Sample flow rate (L/min)	0.2–2	10	10
Sheath flow rate (L/min)	2–20	40	40

instruments like SMPS and CPC. But there is very limited information about the accuracy of the EEPS. In just one of the study, Zervas and Dorlhene [33] compared the exhaust particle number measured by the EEPS with that by the CPC and the Electrical Low Pressure Impactor (ELPI) for a Diesel engine running at steady speeds and New European driving cycle (NEDC). The measurements were conducted for the upstream and downstream of several Diesel Particulate Filters (DPFs). Results show that the three instruments measured quite similar total particle numbers on steady speeds and on the NEDC for the test upstream DPF. For steady speed downstream DPF measurements, CPC and ELPI measured similar results for particle numbers, but EEPS signal was generally below its detection limit. However for steady speed upstream DPF measurement, ELPI and EEPS measured quite similar median diameters but with different shapes of particle size distribution.

The aim of this paper is to investigate the influences of particle morphology on the measured nanoparticle size distributions by the EEPS using the SMPS as the reference. After the calibration check of the EEPS and SMPS using standard Polystyrene Latex spheres (PSL, 3100A, Nanosphere Size Standards, Thermo Scientific, USA), the EEPS and SMPS were challenged with polydisperse silver nanoparticles generated from a tubular furnace for comparing the size distributions. Then monodisperse silver nanoparticles (d_{m2}) of different morphologies, which were classified by the Electrostatic Classifier (EC, TSI, 3080) after the first tubular furnace (d_{m1}) and sintered in the second tubular furnace, were introduced to the EEPS and SMPS for the comparison tests. The theoretical values of the mean charge per agglomerated particle ($N_{p,agg}$) and mean charge per spherical particle ($N_{p,sphere}$) for the silver nanoparticles were calculated based on Fuchs' [34] and Chang's [30] theories with $C_{p,agg}$ obtained from the model of Shin et al. [32], respectively, and compared with the experimental data to determine the accuracy of the d_{m2} measured by the EEPS.

2. Theoretical Background

The unipolar diffusion charging theory for spherical particles [34] and agglomerates [30] is briefly presented in the following, which will be used later to calculate $N_{p,agg}$, $N_{p,sphere}$ and d_{m2} for silver nanoparticles.

2.1. Fuchs' Limiting-Sphere Theory for Spherical Particles

Details about Fuchs' limiting sphere theory were summarized in previous studies [34–36]. The limiting-sphere theory was used to simulate $N_{p,sphere}$ for the unipolar diffusion charger. The birth-and-death theory was used to solve the problem of diffusion charging in unipolar ionized gases as proposed by Boisdron and Brock [37]. According to the theory, the evolution of the charge distribution on monodisperse particles is given by the solution of an infinite set of differential-difference equations (DDEs) as,

$$\frac{dn_{p,0}}{dt} = -\delta_0 n_{p,0} n_i \tag{1}$$

$$\frac{dn_{p,1}}{dt} = \delta_0 n_{p,0} n_i - \delta_1 n_{p,1} n_i \tag{2}$$

$$\vdots$$

$$\frac{dn_{p,n}}{dt} = -\delta_{n-1} n_{p,n-1} n_i - \delta_n n_{p,n} n_i \tag{3}$$

where $n_{p,n}$ is the number concentration of particles with n elementary charges, n_i is the number concentration of ion (#/cm^3), δ_n is the combination coefficient of ions with particles carrying n elementary charges. By solving these infinite set of DDEs, Eqs. (1)–(3), $n_{p,n}$ can be calculated which is then used to calculate $N_{p,sphere}$ as:

$$N_{p,sphere} = \sum_{j=0}^{n} \frac{n_{p,j} \times j}{n_t} \tag{4}$$

where n_t is the total particle concentration (#/cm^3) and the subscript j is the number of elementary charges which ranges from 0 to n.

2.2. Unipolar Diffusion Charging Theory for Non-spherical Particles

Based Chang's [30] diffusion charging theory and Brown and Hemingway's [38] approach for electrical capacitance, Shin et al. [32] developed a new model for the electrical capacitance of agglomerates and calculated $N_{p,agg}$ of silver agglomerates which agreed well with experimental data. In the present study, the same approach as that of Shin et al. [32] was used to predict $N_{p,agg}$. The calculation procedure is briefly presented here. Other details can be found in Shin et al. [32].

The theory of charge deposition on charged aerosol particles of an arbitrary shape developed by Laframboise and Chang [24] was re-examined by Chang [30], who proposed the simpler equations for unipolar diffusion charging process of prolate and oblate spheroids. The mean charge per particle $N_{p,agg}$ for arbitrarily shaped particles obtained from unipolar diffusion charging is governed by the following equations:

$$\sum_{m=1}^{\infty} \left(\frac{\phi_p^m}{m \cdot m!} \right) = \frac{e^2}{kT} \frac{N_i D t}{\varepsilon_0}, \phi_p = \frac{e^2 N_{p,agg}}{C_{p,agg} kT} \left(\phi_p > 1 \right) \tag{5}$$

in continuum regime (ionic Knudsen number, $Kn_{ion} \rightarrow 0$), and

$$N_{\mathrm{p,agg}} = \frac{2C_{\mathrm{p,agg}}kT}{e^2}\ln\left(1 + \frac{e^2 N_{\mathrm{i}}\bar{v}S_{\mathrm{p}}t}{4kTC_{\mathrm{p,agg}}}\right) \quad (6)$$

in free molecule regime ($\mathrm{Kn_{ion}} \rightarrow \infty$). In the above equations, $C_{\mathrm{p,agg}}$ is the electrical capacitance ($\mathrm{C^2/Nm}$), D is the ion diffusion coefficient ($\mathrm{m^2/s}$), e is the elemental electron charge (1.6×10^{-19} C), k is the Boltzmann's constant (1.38×10^{-23} Nm/K), T is the operational gas temperature (K), ε_0 is the permittivity of vacuum ($\mathrm{C^2/Nm^2}$), φ_p is the non-dimensional potential which is equal to $eV/kT = e^2N_{\mathrm{p}}/C_{\mathrm{p}}kT$, $\bar{v}$ is the average ion thermal velocity, N_{i} is the ion concentration in the charger, S_{p} is the geometric surface area, t is the charging time. Equation (5) is used in the present study since it predicts charge per particle which is in good agreement with the experimental data for branched chain agglomerates, the most likely form of silver agglomerates [32].

In Eqs. (5) and (6), $C_{\mathrm{p,agg}}$ is an important parameter to calculate $N_{\mathrm{p,agg}}$. The theoretical approach to calculate $C_{\mathrm{p,agg}}$ is given in Brown and Hemingway [38]. A typical agglomerate is comprised of N primary spheres with the same diameter d_{p} and the center of the sphere i is located at the position vector $\boldsymbol{r_i}$. It is assumed that if a fixed electric charge Q is placed on a conducting agglomerate, it will distribute itself amongst the primary spheres as the own electric charge Q_i at $\boldsymbol{r_i}$ and reduce the electrostatic energy of the agglomerate φ to a minimum. Therefore the electric charge Q and minimum electrostatic energy of the agglomerate φcan be solved by the following equations:

$$\sum_{i=1}^{N} Q_i = Q \quad (7)$$

$$\varphi_s = \sum_{i=1}^{N} \frac{{Q_i}^2}{4\pi\varepsilon_0 d_p} \quad (8)$$

$$\varphi_i = \frac{1}{2}\sum_{i=1}^{N}\sum_{\substack{j=1 \\ i\neq j}}^{N} \frac{Q_i Q_j}{4\pi\varepsilon_0\left|\boldsymbol{r_i} - \boldsymbol{r_j}\right|} \quad (9)$$

$$\frac{\partial}{\partial Q_i}\left[\varphi_l + \varphi_s + k\left(\sum_{i=1}^{N} Q_i - Q\right)\right] = 0 \quad \text{for all } i, \quad (10)$$

where φ_s is the self-energies of all the primary particles, φ_i is pairwise interaction electrostatic energy, k is the Lagrangian multiplier. The minimum electrostatic energy of the agglomerate is obtained by minimizing the electrostatic energy $\varphi = (\varphi_s + \varphi_i)$ with respect to each Q_i subject to the constraints in Eq. (7). Thus, the electrical capacitance of agglomerate is given by the following equations:

$$C_{\mathrm{p,agg}} = \frac{Q^2}{2\varphi} \quad (11)$$

In Eqs. (7)–(10), the number of primary particles N must be found. Lall and Friedlander [39] obtained the following relationship between N, primary particle diameter (d_{p}) and mobility size diameter (d_{m}) as:

$$N = \frac{12\pi\lambda}{c^*{d_{\mathrm{p}}}^2}\frac{d_{\mathrm{m}}}{C_{\mathrm{c}}(d_{\mathrm{m}})}, \quad \text{for } N > 12 \quad (12)$$

where λ is the mean free path, $C_{\mathrm{c}}(d_{\mathrm{m}})$ is the Cunningham slip correction factor, c^* is the dimensionless drag force which depends on particle orientation. In this study, c^* is assumed to be 9.17, which is the value for the agglomerate with random orientation [39].

Like the FMPS, working of the EEPS depends upon the electrical mobility Z_{p} of particles charged by the unipolar diffusion charger. Particles are separated and then deflected to the specified electrometer based on Z_{p} and subsequently be counted [18]. Fuchs' limiting sphere theory was used to predict the probability of particles being detected on a specific channel [34]. Particles with high Z_{p} (small size particles) are deflected to the electrometer near the top of the column, while those with low Z_{p} (large size particles) are deflected further downstream [18, 19]. Z_{p} for an agglomerate or sphere with the equivalent electrical mobility diameter d_{m1} can be calculated as:

$$Z_{\mathrm{p}} = \frac{N_{\mathrm{p}}eC_{\mathrm{c}}(d_{\mathrm{m1}})}{3\pi\mu d_{\mathrm{m1}}} \quad (13)$$

where e is the charge of an electron charge and μ is the dynamic viscosity of the gas.

Based on the theoretical charge per particles for spheres and agglomerate, Eqs. (4) and (5), respectively, the following equation can be used to calculate the theoretical equivalent mobility diameter determined by the EEPS, d_{m2}, when the agglomerates with the initial mobility diameter d_{m1} but different morphologies are introduced into the instrument:

$$\frac{N_{\mathrm{p,agg}}eC_{\mathrm{c}}(d_{\mathrm{m1}})}{3\pi\mu d_{\mathrm{m1}}} = \frac{N_{\mathrm{p,sphere}}eC_{\mathrm{c}}(d_{\mathrm{m2}})}{3\pi\mu d_{\mathrm{m2}}} \quad (14)$$

It is expected that d_{m2} will be smaller than d_{m1} as agglomerates acquire more charges than spheres in the unipolar charger of the EEPS.

3. Experimental Methods

PSL nanoparticles of 100 nm in diameter were generated by atomizing the PSL containing aqueous solution using a constant output atomizer (TSI model 3076) and then classified by the TSI 3080N Electrostatic Classifier (EC) with a nano-DMA (nano Differential Mobility Analyzer, TSI Model 3085). After that, monodisperse PSL particles were measured by the SMPS (TSI Model 3936) equipped with a UWCPC (ultrafine water-based CPC, TSI Model 3786) and the EEPS. Then silver nanoparticles were generated to

study the influence of particle morphology on the size distribution data of the EEPS. The schematic diagram of the experimental setup and experimental conditions are shown in Fig. 1 and Table 2, respectively. Silver powder (purity level 99.9 %, Sigma-Aldrich, USA) was loaded in a ceramic boat in a tube furnace (Lindberg/Blue, Laboratory Tube Furnace CC58114C-1, max temp.: 1,200 °C) and evaporated at the temperature of 1000, 1100 and 1200 °C. Clean air was used as carrier gas with the flow rate of 1.5 lpm. After the furnace, cooling air was used to quench silver vapor to produce silver nanoparticles of high concentration which further grew in the agglomeration chamber. Number distributions of polydisperse silver nanoparticles were then measured by the EEPS and SMPS simultaneously.

For studying the morphology effect, polydispersed silver nanoparticles were introduced into the EC to classify monodisperse particles with the initial mobility diameter d_{m1} of 30, 80, 150, 250 and 350 nm. The sheath and aerosol flow rates for the EC were 9 and 1 lpm, respectively, to ensure high monodispersity. Monodisperse silver particles were then sintered in the second furnace (Lindberg/Blue, Laboratory Tube Furnace STF55433C-1, max temp. 1,500 °C) at the temperature from room temperature (no sintering) to 600 °C to change the morphology of the nanoparticles for comparing the measure mobility diameters (d_{m2}) of the SMPS and EEPS. All measurements were conducted with the time resolution of 135 s for the SMPS and 60 s for the EEPS per one distribution.

Table 2 Experimental conditions

Type	Residence time (s)	Temperature (°C)
1st furnace	2.6	1,150
Agglomeration chamber	270	25
2nd furnace	2.6	25–600

To measure different projected properties and the morphology of monodisperse silver nanoparticles, a home-made concentrated nanoparticles sampler (CNS) was placed after the second furnace for collecting silver nanoparticles. The CNS is modified from the Personal Nanoparticle Sampler (PENS) in which the PCTE filter (Polycarbonate Membrane Filter, PCT-10013100 Sterlitech, USA) was used to replace the impaction plate [40]. The TEM grid (01800-F, Ted Pella, USA) was placed on top of the PCTE filter to collect nanoparticles for subsequent Transmission Electron Microscopy (TEM) analysis.

4. Results and Discussion

For the quality assurance of aerosol measurement, UWCPC was calibrated with Aerosol Electrometer (AE, TSI model 3068) using monodisperse silver nanoparticle of 30 and 60 nm in diameter and the results are shown in Fig. 2. Good agreement between the measured concentrations by the UWCPC and AE (within ±10 % difference) are observed.

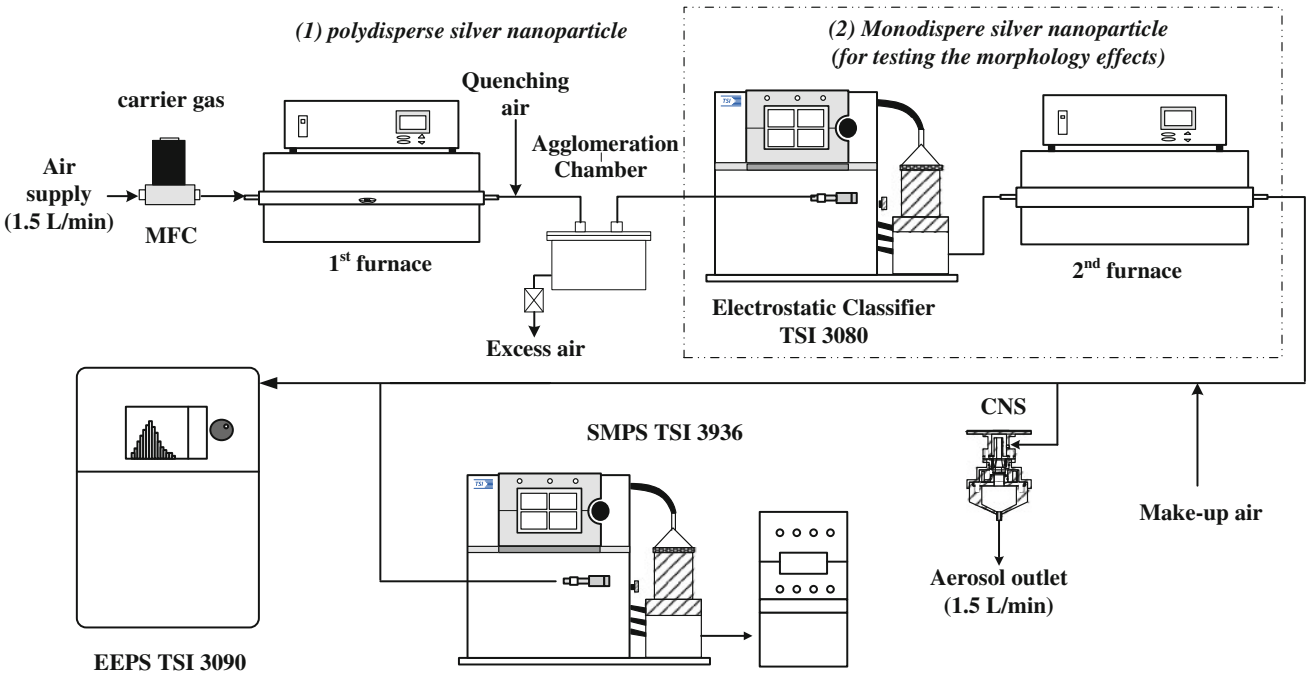

Fig. 1 Experimental setup for the comparison tests of the EEPS and SMPS

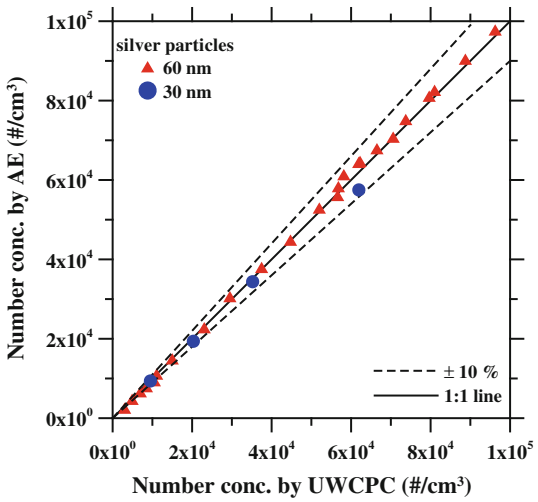

Fig. 2 Calibrated results for the ultrafine condensation particle counter

Figure 3 shows the size distribution of 100 nm PSL particles measured by the EEPS and SMPS. The total particle concentration measured by the EEPS, 785 #/cm^3, is quite different from that by the SMPS, which is 3,520 #/cm^3. The NMDs of the SMPS and EEPS are similar, which are 98.2 and 107.5 nm, respectively, with the deviation of −1.8 and +7.5 % from the nominal diameter of 100 nm. The polydispersity of 100 nm PSL particles is observed for the EEPS, which was also shown in a TSI report for the FMPS that a monodisperse particle will spread over 5 channels and is not suitable for monodisperse particle measurements (ftp://ftp.tsi.com/pub/Lo_Charles/SOP%20-%20good%20practice-TJ.pdf).

4.1. Polydisperse Silver Agglomerates

After the calibration check, the EEPS and SMPS were used to measure polydisperse silver nanoparticles for comparing the size distributions. For the first furnace temperature of 1000, 1100 and 1200 °C, Fig. 4 shows that the total concentrations of the EEPS (1.29×10^5, 8.33×10^5 and 4.87×10^6 #/cm^3, respectively) is higher than the SMPS (7.78×10^4, 4.99×10^5 and 3.3×10^6 #/cm^3, respectively), with the maximum relative difference up to 67 %. The EEPS shows smaller NMDs (7.29 ± 0.1, 8.24 ± 0.02 and 25.2 ± 0.49 nm) in comparison to the SMPS (8.11 ± 0.02, 8.37 ± 0.05 and 31.82 ± 0.498 nm) at the temperature of 1000, 1100 and 1200 °C, respectively with a maximum relative difference up to 21 %. In previous studies [21–23], the FMPS was also shown to measure smaller NMDs in comparison to the SMPS for soot and TiO_2 agglomerates. However the definite reason was yet to be found. Hence the monodisperse silver nanoparticles sintered in the second tubular furnace were measured by the SMPS and EEPS to study the effect of morphology on the measured d_{m2}.

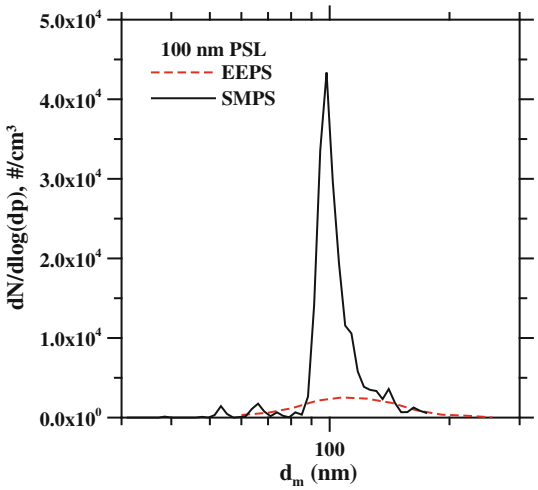

Fig. 3 The size distribution of 100 nm PSL particles measured by the EEPS and SMPS

4.2. Monodisperse Silver Agglomerates

Figure 5 shows the variation of measured d_{m2} by the EEPS and SMPS for monodisperse silver nanoparticles of d_{m1} versus sintering temperature. For both instruments, d_{m2} decreases drastically at any d_{m1} when the sintering temperature is increased from room temperature (no sintering) to 200 °C, and then it approaches a constant value when the sintering temperature is greater than 200 (for d_{m1} <150 nm) or 400 °C (for d_{m1} >250 nm) as particles become nearly spherical. At room temperature to 600 °C, no difference is observed between d_{m2} of the SMPS and EEPS for d_{m1} of 30 nm. For particles of larger sizes i.e., d_{m1} = 80–300 nm, difference between d_{m2} of the SMPS

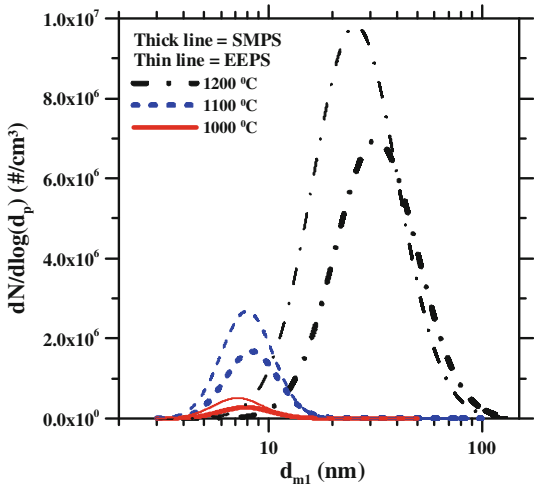

Fig. 4 The size distributions of polydisperse silver nanoparticles measured by the SMPS and EEPS at different generation temperatures at the first furnace

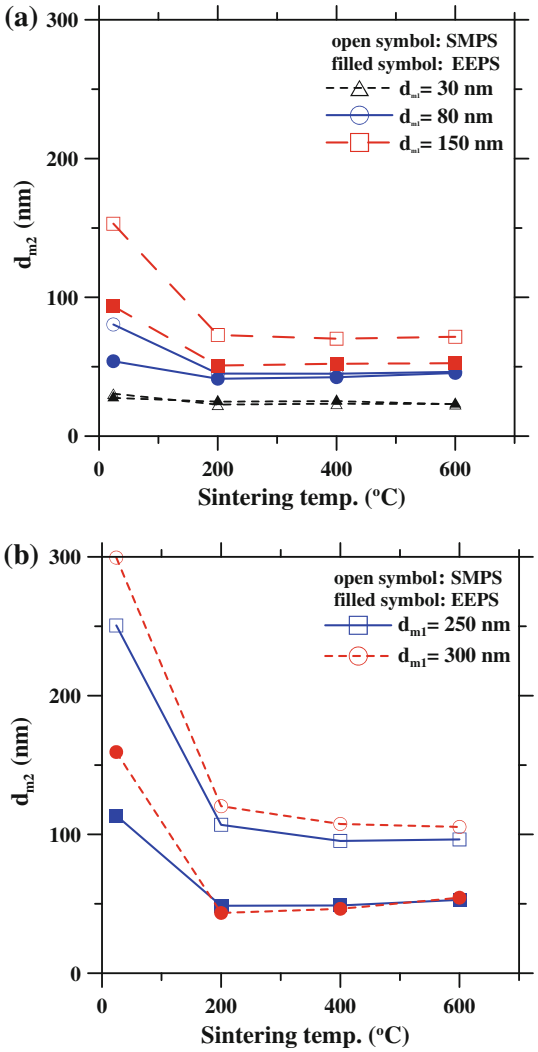

Fig. 5 The variation of measured d_{m2} by the SMPS and EEPS for monodisperse silver nanoparticles with different initial d_{m1} versus sintering temperature. **a** $d_{m1} = 30$, 80, 150 nm, **b** $d_{m1} = 250$, 300 nm

and EEPS is observed with the maximum occurring at room temperature and then the difference decreases with increasing sintering temperature from room temperature to 200 °C. When d_{m1} is larger than 150 nm, the difference persists in d_{m2} even when the sintering temperature is increased from 200 to 600 °C.

The size distributions measured by the EEPS and SMPS for monodisperse silver nanoparticles with different initial mobility diameters (d_{m1}) are compared in Fig. 6 without sintering. The distribution observed in the SMPS is nearly monodisperse while polydispersity is observed in the EEPS, similar to that observed for monodisperse PSL particles. Note that the second peaks in the SMPS data are due to doubly charged particles. The NMD of the EEPS, which is 54.0, 93.5, 113.6 and 159.3 nm in (a)–(d), respectively) is seen to be much smaller than that of the SMPS, which is 80, 150, 250 and 300 nm in (a)–(d), respectively, as in the case of polydisperse silver nanoparticles. The total particle concentrations of the EEPS are 2–3 times those of the SMPS. These data further indicate that the EEPS is not designed for monodisperse particle measurements as stated in the TSI report (ftp://ftp.tsi.com/pub/Lo_Charles/SOP%20-%20good%20practice-TJ.pdf).

TEM images of monodisperse silver nanoparticles of different sizes are shown in Fig. 7. It is observed that without sintering, silver nanoparticles of different sizes are loose agglomerates. The shape of small silver agglomerates ($d_{m1} = 30$ and 80 nm) is changed from chain agglomerates to nearly spherical particles at the sintering temperature of 200 °C. Whereas, the shape of large silver agglomerates ($d_{m1} = 250$ and 300 nm) is gradually changed from chain agglomerates to oblate spheroids with increasing sintering temperature. These images help to explain why the difference in d_{m2} between the EEPS and SMPS under no sintering condition exists only for particles larger than 80 nm at room temperature while the difference decreases as sintering temperature is increased to 600 °C as shown in Fig. 5. When d_{m1} is larger than 150 nm, the difference still persists in d_{m2} even at the sintering temperature of 600 °C because the particles are still not perfect spheres but remain to be oblate spheroids as observed in (g)–(l) of Fig. 7.

4.3. Quantitative Explanation for the Differences Observed in Size Measurements

The above results demonstrate that the measured size distribution data of the EEPS is influenced by the morphology of the silver nanoparticles. To find the quantitative reason that why silver agglomerates measured by the EEPS have smaller d_{m2} as shown in Fig. 6, theoretical $N_{p,agg}$ was calculated based on the theory shown in the previous section. For the calculation, the projected properties of silver agglomerates seen as branched chain agglomerates have to be determined, including the primary particle diameter (d_p), the maximum projected length (L), the maximum projected width (W) and aspect ratio ($\beta = L/W$). These parameters were obtained from the TEM images analyzed using the Image J 1.46 K software (National Institutes of Health, USA). A typical TEM image of agglomerates with the indicated parameters is shown in Fig. 8. Table 3 shows the average projected properties of the monodisperse silver agglomerates with d_{m1} from 80 to 300 nm. It is seen that primary particle size is not constant but is increased from 12.33 to 14.64 nm as d_{m1} is increased from 80 to 300 nm. The average β values increases from 1.7 to 1.93 as d_{m1} is increased from 80 to 300 nm. The average β values for d_{m1} of 80 and 150 nm are 1.70 ± 0.55 and 1.71 ± 0.41, respectively, which are slightly smaller than 1.77 ± 0.56 and 1.79 ± 0.51 shown in Shin et al. [41].

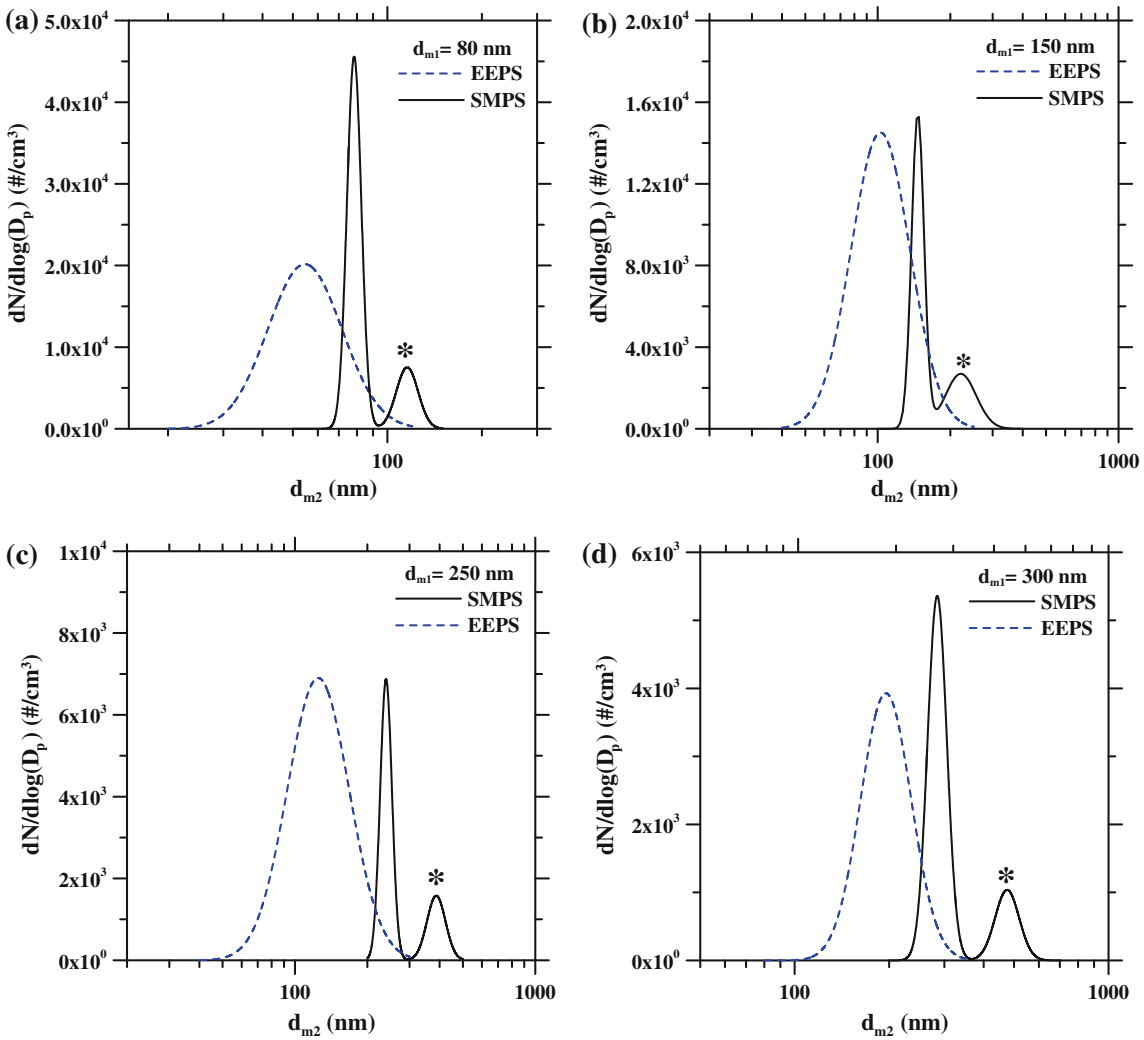

Fig. 6 The size distributions of monodisperse silver nanoparticles measured by the EEPS and SMPS for different initial values of d_{m1} at room temperature (no sintering). *Note* Second peak marked by *asterisk* in the SMPS data are due to doubly charged particles

Using these parameters, $N_{p,agg}$ and $N_{p,sphere}$ of silver nanoparticles were calculated and compared. The results are shown in Fig. 9 in which $N_{p,agg}$ is found to be larger than $N_{p,sphere}$ and the difference increases as d_{m1} is increased. Similar results were obtained by Shin et al. [34] who observed that the mean charge per particle for silver agglomerates was 24 % higher than that of silver spheres.

Figure 10 shows the variation of calculated Z_p for agglomerates and spheres as a function of d_{m1}. As they acquire higher particle charges in the charger, silver agglomerates will have higher Z_p values than those of spherical particles of the same d_{m1} and the difference slightly increases with increasing d_{m1} as shown in the figure. Since the working of the EEPS depends on Z_p, the EEPS will underestimate the mobility diameter of agglomerates.

The results of calculated and measured d_{m2} for silver agglomerates as a function of d_{m1} are shown in Fig. 11. It is seen that the measured d_{m2} values agree well with the experimental data with the difference of 16.69, −9.09, −6.69 and −5.84 % for d_{m1} of 80, 150, 250 and 300 nm, respectively. A large variation of calculated d_{m2} is due to the large SD in β (Table 3) which was also observed in Shin et al. [41].

5. Conclusion

The fast mobility particle sizer such as the Engine Exhaust Particle Sizer Spectrometer investigated in this study is a very useful nanoparticle monitoring device. This study focuses on its measurement accuracy in size distributions using the commonly used TSI SMPS as the reference. For polydisperse silver agglomerates, the EEPS shows higher total number concentrations with a maximum relative difference up to 67 % and consistently smaller number median mobility diameters in comparison to the SMPS. For monodisperse silver nanoparticles, the EEPS shows

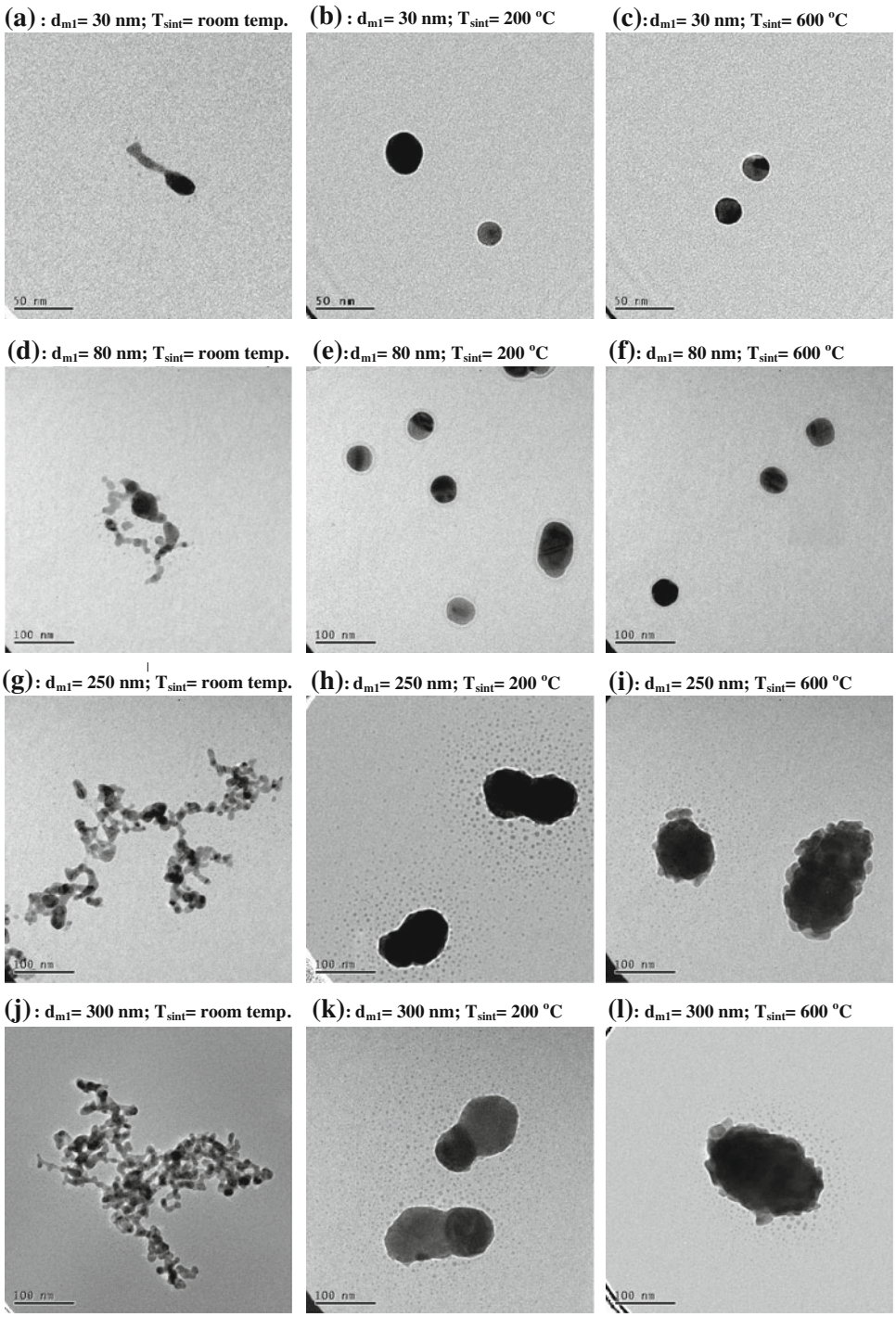

Fig. 7 Representative TEM images of different size silver nanoparticles at different sintering temperatures. **a–c** $d_{m1} = 30$ nm; **d–f** $d_{m1} = 80$ nm; **g–i** $d_{m1} = 250$ nm; **j–l** $d_{m1} = 300$ nm

polydispersity with smaller median diameters for particles with the mobility diameter larger than 80 nm as particles spread over several channels. For smaller silver agglomerates (<80 nm) as well as PSL spheres, the NMDs of the EEPS are close to those of the SMPS as particles are more compact. These results are consistent with the manufacturer's report that the instrument is not intended for monodisperse particle measurement.

With the current knowledge of the unipolar diffusion charging theories of agglomerates, it is demonstrated that predicting the theoretical response of the EEPS in mobility diameter with respect to nanoparticles of different morphologies is possible. The current study shows the predicted mobility diameters of the EEPS are close to those of the measured values when the monodisperse silver nanoparticles of known mobility diameter and morphology are

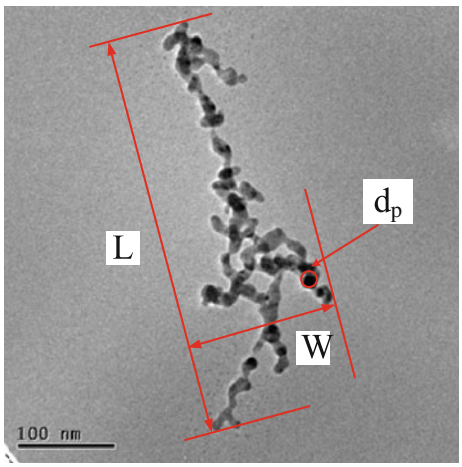

Fig. 8 Parameters of agglomerates from TEM images

Table 3 Projected properties of silver agglomerates for $d_{m1} = 80$, 150, 250, 300 nm

d_{m1} (nm)	n	d_p (nm)	β (L/W)
80	49	12.33 ± 3.70	1.70 ± 0.55
150	85	12.80 ± 3.49	1.71 ± 0.41
250	121	13.82 ± 4.19	1.84 ± 0.44
300	57	14.64 ± 6.57	1.93 ± 0.51

Data are presented as mean ± SD; n No. of analyzed agglomerates

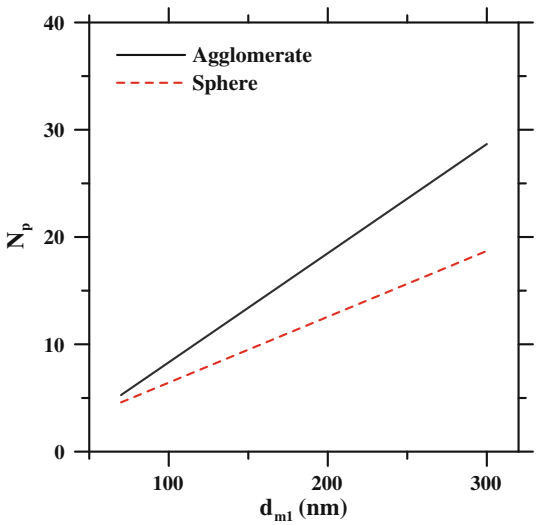

Fig. 9 The mean charge per particle $N_{p,agg}$ and $N_{p,sphere}$ as a function of the initial mobility diameter d_{m1}

monitored. Although quantitative explanation of the reason for underestimation of the mobility diameter is shown here, it will be worthwhile in the future to better understand the fundamental charging process of the instrument in response to different types and size of nanoparticles, and provide careful calibration of the instrument for monitoring accuracy in both particle size and concentration.

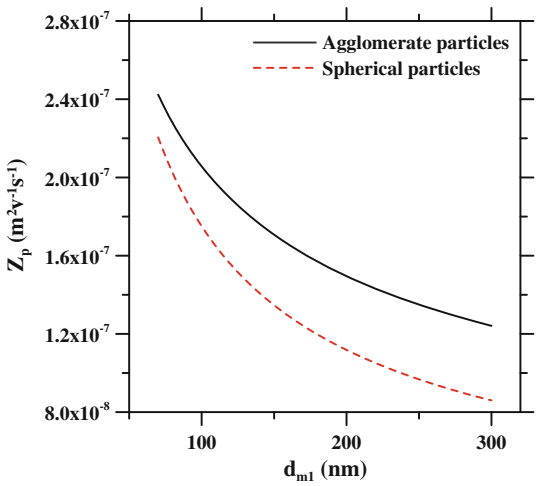

Fig. 10 The variation of calculated Z_p for agglomerates and spheres as a function of the initial mobility diameter d_{m1}

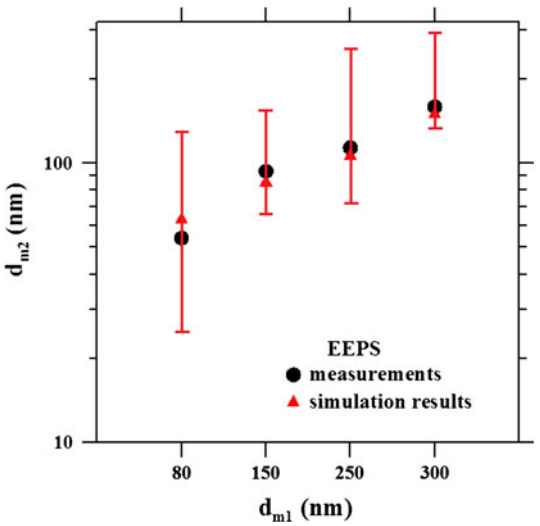

Fig. 11 The comparison of simulated and measured d_{m2} by the EEPS as a function of the initial mobility diameter d_{m1}. Large variation of the simulated d_{m2} is due to the large SD of the aspect ratio

Acknowledgments The financial support of Taiwan Institute of Occupational Safety and Health (project number IOSH 101-H324) is gratefully acknowledged.

References

[1] K. Donaldson, D. Brown, A. Clouter, R. Duffin, W. MacNee, L. Renwick, L. Tran and V. Stone, The pulmonary toxicology of ultrafine particles, J. Aerosol Med., **15**(2002) 213–220.
[2] G. Oberdorster, E. Oberdorster and J. Oberdorster, Nanotoxicology: an emerging discipline evolving from studies of ultrafine particles, Environ. Health Perspect., **113**(2005) 823–839.
[3] Z. Magdolenova, D. Bilanicova, G. Pojana, L. M. Fjellsb, A. Hudecova, K. Hasplova, A. Marcomini and M. Dusinska, Impact of agglomeration and different dispersions of titanium dioxide nanoparticles on the human related in vitro cytotoxicity and genotoxicity, J. Environ. Monit., **14**(2012) 455–464.

[4] Y. Thomassen, W. Koch, W. Dunkhorst, D. G. Ellingsen, N. Skaugset, L. Jordbekken, P. A. Drablos and S. Weinbruch, Ultrafine particles at workplaces of a primary aluminium smelter, J. Environ. Monit., **11**(2009) 2077–2086.
[5] B. K. Ku and A. D. Maynard, Generation and investigation of airborne silver nanoparticles with specific size and morphology by homogeneous nucleation, coagulation and sintering, J. Aerosol Sci., **37**(2006) 452–470.
[6] A. A. Lall, M. Seipenbusch and S. K. Friedlander, On-line measurement of ultrafine aggregate surface area and volume distributions by electrical mobility analysis: II. Comparison of measurements and theory, J. Aerosol Sci., **37**(2006) 272–282.
[7] S. G. Aggarwal, Recent developments in aerosol measurement techniques and metrological issues, MAPAN, **25**(2010) 165–189.
[8] R. C. Flagan, History of electrical aerosol measurements, Aerosol Sci. Technol., **28**(1998) 301–380.
[9] P. A. Baron and K. Willeke, Aerosol measurement: principle, technique and applications, 2nd Ed., Jon Wiley & Sons Inc., (2001) 537–568.
[10] S. C. Chen, C. J. Tsai, C. Y. Huang, H. D. Chen, S. J. Chen, C. C. Lin, J. H. Tsai, C. C. K. Chou, S. C. C. Lung, W. R. Huang, G. D. Roam, W. Y. Wu, J. Smolik and L. Dzumbova, Chemical mass closure and chemical characteristics of ambient ultrafine particles and other PM fractions, Aerosol Sci. Technol., **44**(2010) 713–723.
[11] S. C. Chen, C. J. Tsai, C. C. K. Chou, G. D. Roam, S. S. Cheng and Y. N. Wang, Ultrafine particles at three different sampling locations in Taiwan, Atmos. Environ., **44**(2010) 533–540.
[12] Y. H. Cheng, C. H. Huang, H. L. Huang and C. J.Tsai, Concentrations of ultrafine particles at a highway toll collection booth and exposure implications for toll collectors, Sci. Total Environ., **409**(2010) 364–369.
[13] C. J. Tsai, C. Y. Huang, S. C. Chen, C. E. Ho, C. H. Huang, C. W. Chen, C. P. Chang, S. J. Tsai and M. J. Ellenbecker, Exposure assessment of nano-sized and respirable particles at different workplaces, J. Nanopart. Res., **13**(2011) 4161–4172.
[14] C. J. Tsai, G. Y. Lin, C. N. Liu, C. E. He and C. W. Chen, Characteristic of nanoparticles generated from different nanopowders by using different dispersion methods, J. Nanopart. Res., **14**(2012) 777–788.
[15] G. Biskos, E. Mastorakos and N. Collings, Monte–Carlo simulation of unipolar diffusion charging for spherical and nonspherical particles, J. Aerosol. Sci., **35**(2004) 707–730.
[16] C. Qi, D. R. Chen and P. Greenberg, Performance study of a unipolar aerosol mini-charger for a personal nanoparticle sizer, J. Aerosol Sci., **39**(2008) 450–459.
[17] H. Tammet, A. Mirme and E. Tamm, Electrical aerosol spectrometer of Tartu University, Atmos. Res., **62**(2002) 15–324.
[18] TSI, Engine Exhaust Particle Sizer Spectrometer; Operation and Service Manual, TSI Incorporated, Shoreview (2005).
[19] TSI, Fast Mobility Particle Sizer Spectrometer; Operation and Service Manual, TSI Incorporated, Shoreview (2006).
[20] H. Kaminski, T. A. J. kuhlbuch, S. Rath, U. Gotz, M. Sprenger, D. Wels, J. Polloczek, V. Bachmann, N. Dziurowitz, H-J. Kiesling, A. Schwiegelshohn, C. Monz, D. Dahmann, and C. Asbach, Comparability of mobility particle sizers and diffusion chargers, J. Aerosol Sci., **57**(2013) 156–178.
[21] C. Asbach, H. Kaminski, H. Fissan, C. Monz, D. Dahmann, S. Miihopt, H. R. Paur, H. J. Kiesling, F. Herrmann, M. Voetz and T. A. J. Kuhlbusch, Comparison of four mobility particle sizers with different time resolution for stationary exposure measurements, J. Nanopart. Res., **11**(2009) 1593–1609.
[22] J. Leskinen, J. Joutsensaari, J. Lyyranen, J. Koivisto, J. Ruusunen, M. Jarvela, T. Tuomi, K. Hameri, A. Auvinen and J. Jokiniemi, Comparison of nanoparticle measurement instruments for occupational health applications, J. Nanopart. Res., **14**(2012) 718–733.
[23] C. H. Joeng and G. J. Evans, Inter-comparison of a fast mobility particle sizer and a scanning mobility particle sizer incorporating an ultrafine water-based condensation particle counter, Aerosol Sci. Technol., **43**(2009) 364–373.
[24] J. G. Laframboise and J. S. Chang, Theory of charge deposition on charged aerosol particles of arbitrary shape, J. Aerosol. Sci., **8**(1977) 331–338.
[25] R. J. Han and J. W. Gentry, Evolution of charge distributions of non-spherical particles undergoing unipolar charging, J. Aerosol. Sci., **25**(1994) 499–508.
[26] B. P. Frank, S. Sltiel, O. Hogrefe, J. Grygas and G. G. Lala, Determination of mean particle size using the electrical aerosol detector and the condensation particle counter: comparison with the scanning mobility particle sizer, J. Aerosol Sci., **39**(2008) 19–29.
[27] S.N. Rogak, and R.C. Flagan, Bipolar diffusion charging of spheres and agglomerate aerosol particles, J. Aerosol Sci., **23**(1992) 693–710.
[28] S. N. Rogak, R. C. Flagan, and H. V. Nguyen, The mobility and structure of aerosol agglomerates, Aerosol Sci. Technol., **18**(1993) 25–47.
[29] A. Keller, M. Fierz, K. SiegMann, H. C. Siegmann and A. Filippov, Surface science with nanosized particles in a carrier gas, J. Vac. Sci. Technol., **19**(2001) 1–8.
[30] J. S. Chang, Theory of diffusion charging of arbitrarily shaped conductive aerosol particles by unipolar ions, J. Aerosol Sci., **12**(1981) 19–26.
[31] H. Oh, H. Park and S. Kim, Effects of particle shape on the unipolar diffusion charging of nonspherical particles, Aerosol Sci. Technol., **38**(2004) 1045–1053.
[32] W. G. Shin, J. Wang, M. Mertler, B. Sachweh, H. Fissan and D. Y. H. Pui, The effect of particle morphology on unipolar diffusion charging of nanoparticle agglomerates in the transition regime, J. Aerosol Sci., **41**(2010) 975–986.
[33] E. Zervas, and P. Dorlhene, Comparison of exhaust particle number measured by EEPS, CPC, and ELPI, Aerosol Sci. Technol., **40**(2006) 977–984.
[34] N. A. Fuchs, On the stationary charge distribution on aerosol particles in bipolar ionic atomosphere, Pure Appl. Geophys., **56**(1963) 185–193.
[35] G. Biskos, K. Reavell and N. Collings, Unipolar diffusion charging of aerosol particles in the transition regime, J. Aerosol Sci., **36**(2005) 247–265.
[36] F. J. Romay and D. Y. H. Pui, Free electron charging of ultrafine aerosol particles, J. Aerosol Sci., **23**(1992) 679–692.
[37] K. Boisdron and J. R. Brock, On the stochastic nature of the acquisition of electrical charge and radioactivity by aerosol particles, Atmos. Environ., **4**(1970) 35–50.
[38] R. C. Brown and M. A. Hemingway, Electric charge distribution and capacitance of agglomerates of spherical particles: theory and experimental simulation, J. Aerosol Sci., **26**(1995) 1197–1206.
[39] A. A. Lall and S. K. Friedlander, On-line measurement of ultrafine aggregate surface area and volume distributions by electrical mobility analysis: I. Theoretical analysis, J. Aerosol Sci., **37**(2006) 260–271.
[40] C. J. Tsai, C. N. Liu, S. M. Hung, S. C. Chen, S. N. Uang, Y. S. Cheng and Y. Zhou, Novel active personal nanoparticle sampler for the exposure assessment of nanoparticles in workplaces, Environ. Sci. Technol., **46**(2012) 4546–4552.
[41] W. G. Shin, J. Wang, H. Fissan and D. Y. H. Pui, Structural properties of silver nanoparticle agglomerates based on transmission electron microscopy: relationship to particle mobility analysis, J. Nanopart. Res., **11**(2009) 163–173.